Journal of Current Research in Oral Surgery
2026, Volume 6, Issue 1, Page No: 10-16

Available online at: www.tsdp.net

ISSN: 3062-3480

Original Article

Finite Element Evaluation of Thread Depth Influence across Four Implant Thread Designs on Bone–Implant Stress Distribution: A 3D in Vitro Study

Emily Johnson[1]*, Robert Smith[1], Laura Brown[2], Kevin Miller[1]

[1]Department of Oral Surgery and Dental Implantology, Faculty of Dentistry, University of Toronto, Toronto, Canada.
[2]Department of Maxillofacial Clinical Sciences, Faculty of Medicine and Dentistry, McGill University, Montreal, Canada.

***E-mail** ✉ emily.johnson@gmail.com

Received: 28 September 2025; **Revised:** 12 January 2025; **Accepted:** 14 January 2026

ABSTRACT

The favorable outcomes of dental implant rehabilitation are predominantly rooted in the creation and long-term preservation of an osseointegrated junction between bone and implant. Multiple variables shape the formation of this junction, among which the implant thread architecture exerts a paramount influence. The objective of this work is to examine how thread depth, assessed across four separate thread configurations, affects stress distribution at the bone-implant boundary using three-dimensional finite element modeling. Four distinct implant geometries were engineered, differing in thread profile—V thread, square thread, buttress thread, and reverse buttress thread—each standardized to a thread depth of 0.4 mm. These geometrical representations were virtually inserted into the mandibular first molar site. Loading was delivered at 100 N along the implant's long axis and obliquely at a 45° inclination. The resultant Von Mises stresses were quantified around the implant–bone contact zone and evaluated across the different configurations. The resultant color-coded stress maps were inspected, and the highest Von Mises stress values were extracted and systematically tabulated for every loading state. Stress dispersal in the computational models is displayed both as numerical outputs and via color gradients. Peak Von Mises stress magnitudes correspond to the red end of the spectrum, whereas minima appear as blue. Intermediate intensities are sequentially represented by bluish green, green, greenish yellow, and yellowish red as stress levels rise. Thread architecture is a critical determinant of stress distribution throughout the implant and adjacent bone. Distinct Von Mises stress magnitudes manifest at the interface zones of cortical bone-implant and cancellous bone-implant. For implant longevity, sound osseointegration is indispensable, and thread geometry is a pivotal contributor. Hence, selecting fixtures with an optimal thread pattern significantly improves the prognosis of an implant-retained restoration.

Keywords: Cortical bone, Implant, Von Mises stress, Osseointegration

How to Cite This Article: Johnson E, Smith R, Brown L, Miller K. Finite Element Evaluation of Thread Depth Influence across Four Implant Thread Designs on Bone–Implant Stress Distribution: A 3D in Vitro Study. J Curr Res Oral Surg. 2026;6(1):10-6. https://doi.org/10.51847/gMqL2tSjag

Introduction

Restoring masticatory function with dental implants constitutes a highly efficacious and foreseeable modality for anchoring oral prostheses. The procedure's foundation rests firmly on the capacity to establish and sustain a direct, osseointegrated bone-implant linkage [1]. A multitude of elements govern this biological fusion, with the macro-design feature of thread configuration being particularly consequential. Accumulated experimental and clinical evidence over decades consistently identifies the most coronal thread as the locus of maximal stress concentration, thereby predisposing this region to initial microfracture and the resultant formation of immature osseointegration. Commercial implant systems exhibit considerable diversity in their thread morphologies. Contemporary scholarly inquiry has focused on elucidating the relative impact and parametric sensitivity of design attributes such as thread pitch, depth, width, and helix

angle. Gaining a thorough grasp of these variables and their judicious application in implantology can substantially mitigate the risk of biomechanical failure. Computational simulation via finite element analysis (FEA) furnishes a robust and meaningful adjunct to conventional clinical and in vivo/vitro experimentation. Employing FEA methodologies to gauge parametric sensitivities constitutes a well-validated application [2]. Within implant dentistry, the finite element (FE) technique has been harnessed to foretell stress distribution contours at the bone-implant boundary—both for comparative assessments of disparate root-form geometries and for replicating an array of clinical scenarios and prosthetic superstructures. A principal merit of this technique lies in its capability to deconstruct intricate structural quandaries into finite, interconnected, simplified segments amenable to mathematical resolution.

Materials and Methods

Procedural sequence of the investigation

The digital modeling of implant fixtures was performed at Tejvi Techno-Solutions, Bangalore, on a computing platform equipped with a Pentium IV processor, 256 MB of RAM, and 80 GB of storage. The ANSYS simulation suite, release 14.5, served as the finite element solver. The virtual implantation was prescribed to the mandibular first molar territory, with computational constructs generated to mirror the in vivo anatomical milieu with high fidelity.

Finite element modeling

Construction of geometric model

Modeling of the bone

A computed tomography (CT) dataset of a normal human mandible from a male subject approximately 26 years of age, lacking any history of implant insertion or mandibular pathology, was procured utilizing a Siemens CT Scanner (Emotion 6 series). The acquisition zone was specified above the cranial vertex, with 0.5-mm slice intervals along the superior-inferior axis, which aligns with the Z-direction in the global coordinate system. The scanning range was extended to capture the soft-tissue contour overlying the inferior mandibular boundary **(Figure 1)**. From this dataset, a portion of the mandible corresponding to the first molar location was isolated to construct the osseous model. The imaging data were then rendered into a three-dimensional volumetric reconstruction of the lower molar territory to facilitate computational evaluation **(Figure 2)**.

Figure 1. CT scan of the mandible

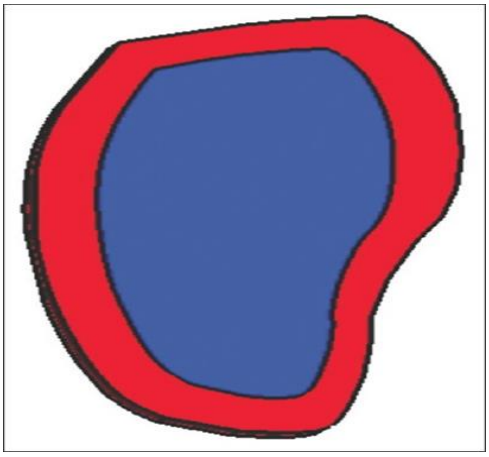

Figure 2. 3D solid model of the lower molar region

Modeling of the implants

Volumetric FE models of the implant assemblies were generated in CATIA. The implants were dimensioned at 10 mm in length and 4 mm in diameter. A standardized thread depth of 0.4 mm was maintained across all four thread profiles under investigation: V-thread, square thread, buttress thread, and reverse buttress thread **(Figure 3)**. The virtual placement of the implant was centered within the mandibular molar site, midway along both the mesio-distal and bucco-lingual dimensions of the toothless span.

a) b)

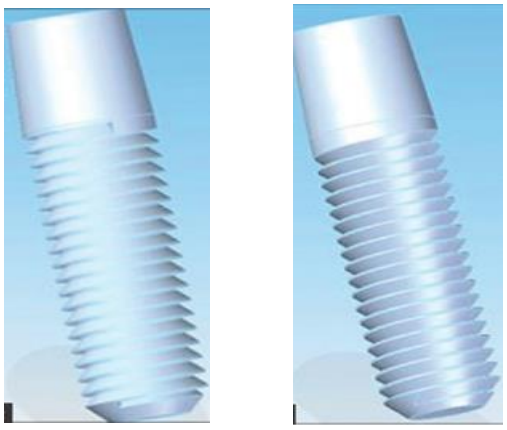

c) d)

Figure 3. (a) V thread, (b) Square thread, (c) Buttress thread, and (d) Reverse buttress thread design

Modeling of the interface

The implants were conceived as threaded, solid machined cores. The 0.4 mm thread depth was selected to facilitate osseous in-growth. Owing to the very fine pitch applied in the model, direct geometric representation of this feature was unworkable; therefore, an equivalent suite of interfacial characteristics was engineered. A stratum of slender interface elements was inserted between the implant exterior and the surrounding bone to emulate the interfacial zone characteristic of bone ingrowth. Based on the investigations by Cook *et al*. [3], it was assumed that the osseous tissue within the porous implant coating at the interface could be approximated as an array of miniature cantilever beams. Translating this concept to the FE construct, each interface element was treated as a prismatic rectangular cantilever beam of constant cross-section spanning between the implant and the bone [3-5].

Mesh generation

The volumetric FE mesh corresponding to the geometric construct was generated using the Ansys Preprocessor (ANSYS version 14.5). A free meshing scheme was adopted owing to the lack of geometric symmetry in the model **(Figure 4)**. Element sizing (SOLID 187) followed the program's default specifications. The element formulation used for this analysis was a 10-node tetrahedral element, with 3 translational degrees of freedom at each node—specifically, displacements along the x, y, and z axes. Elements were formulated to maintain a size-to-aspect-ratio conducive to adequate solution fidelity **(Table 1)**.

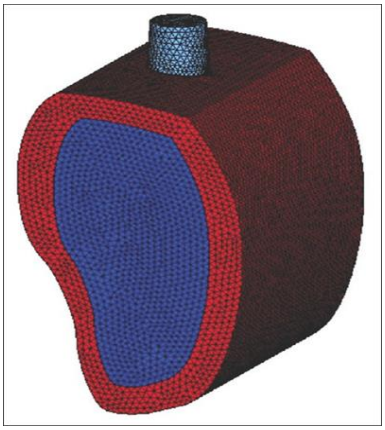

Figure 4. 3D finite element meshed model.

Table 1. Mechanical properties of different materials used in the model

Material type	Elastic modulus (MPa)	Poisson's ratio
Cortical bone tissue	13,700	0.30
Cancellous (trabecular) bone	1370	0.30
Titanium alloy implant	110,000	0.35

Specifying material properties

To facilitate program execution, rigorous analysis, and subsequent interpretation of findings, two material constants were assigned: Young's modulus and Poisson's ratio **(Table 2)**. The cortical bone layer, the cancellous bone core, and the implant-abutment complex were idealized as linearly elastic, homogeneous, and isotropic continua. Despite cortical bone possessing inherent anisotropic material characteristics and site-dependent stiffness heterogeneity, an isotropic simplification was employed due to the paucity of exhaustive data and the challenge of reliably orienting the principal material axes. The mechanical descriptors for the interface substance (osseous tissue integrated into the porous implant coat) were derived computationally under the assumption that it behaves as a composite material. The effective Young's modulus for this composite was calculated as a function of the elastic moduli and volumetric proportions of the implant substance and the bone.

Table 2. Number of elements and nodes

Model type	Total elements	Total nodes
V-shaped thread configuration	431,186	74,190
Square thread configuration	779,086	144,914
Buttress thread configuration	253,653	47,504
Reverse buttress thread configuration	735,035	128,458

Applying boundary conditions

Kinematic constraints were enforced on the distal boundary of the model in all three coordinate directions, while the basal aspect was left unsupported, thereby permitting flexure of the construct. These provisions render the model a more clinically authentic analog.

Application of loads

In vivo investigations have reported masticatory forces ranging from 64 to 720 N, which fluctuate with the type of prosthesis anchored by the implants. Abstracting from the full complexity of masticatory biomechanics, the effect of occlusal force was represented by a 100 N load applied to the abutment at a 45° inclination from the implant long axis in the buccolingual plane. This angulated force was resolved into orthogonal vertical and lateral constituents. The analysis was initially performed for the vertically directed component, with symmetry constraints applied to both the mesiodistal and buccolingual symmetry planes. Upon introducing the lateral force vector, the kinematic conditions on the mesiodistal and buccolingual planes were switched to antisymmetry and symmetry, respectively. In both loading cases, the osseous region was fully immobilized across all degrees of freedom at the distal buccolingual boundary. The net solution was ultimately constructed by superposing these two component analyses. The force magnitude fell within normal physiological parameters, and the orientation of its application mirrored authentic clinical circumstances.

A force of 100 N, delivered both axially and obliquely (at 45°), was directly administered to the abutment of each of the four implant configurations: V thread, square thread, buttress thread, and reverse buttress thread **(Figure 5)**.

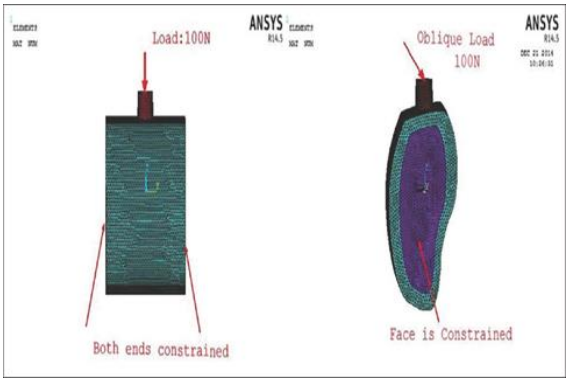

Figure 5. Application of vertical and oblique loads onto the abutment

Finite element analysis

These separate computational models were processed numerically using the solver module, with the resulting outputs displayed in the postprocessor environment of the FE code (Ansys, version 14.5) as color-contoured stress maps using the Von Mises stress criterion.

Von Mises stress magnitudes demarcate the threshold for incipient plastic flow in ductile solids. Structural failure of a metallic implant ensues when the Von Mises stress state exceeds the material's yield point. In the FEA literature, Von Mises stress is the predominant scalar metric used to capture multiaxial stress at a discrete location, making it crucial for evaluating stress regimes developing within the implant body.

Stress patterns in the FE constructs are conveyed both as quantitative readouts and through chromatic mapping, wherein the highest Von Mises intensities correspond to red and the lowest to blue.

Table 1 catalogs the global Von Mises stress and its partitioning within the cortical bone, cancellous bone, and implant under a 100 N vertically oriented load.

Table 2 catalogs the global Von Mises stress and its partitioning within the cortical bone, cancellous bone, and implant under a 100 N oblique (45°) load.

Ethical clearance statement

Institutional ethical sanction for the present study was conferred by Awadh Dental College and Hospital, Jamshedpur, India, dated 11/4/22, under protocol number 218.

Results and Discussion

A set of four volumetric FE models was developed according to the previously delineated design parameters and subsequently investigated under a standardized loading regime in which the vertically intrusive, non-axially directed loads were each set to 100 N. The resulting color-contour plots were systematically scrutinized, and the peak Von Mises stress was extracted and tabulated for each test scenario.

Stress patterns in the FE constructs are conveyed both as quantitative readouts and through chromatic mapping, wherein the highest Von Mises intensities correspond to red and the lowest to blue. Intermediate stress tiers, in order of increasing magnitude, are depicted as bluish green, green, greenish yellow, and yellowish red.

Table 3 catalogs the global Von Mises stress and its partitioning within the cortical bone, cancellous bone, and implant under a 100 N vertically oriented load.

Table 4 catalogs the global Von Mises stress and its partitioning within the cortical bone, cancellous bone, and implant under a 100 N oblique (45°) load.

Table 3. Von Mises stress values (MPa) under 100 N vertical loading

Region of measurement	V-shaped thread	Square thread	Buttress thread	Reverse buttress thread
Cortical bone–implant interface	8.8194	9.30328	9.43991	8.26554
Cancellous bone–implant interface	2.05786	1.20457	1.02297	2.4337
Implant body	16.309	17.6049	17.8409	16.9331
Overall stress	19.451	17.6049	17.8409	16.9331

Table 4. Von Mises stress values (MPa) under 100 N oblique loading (45°)

Region of measurement	V-shaped thread	Square thread	Buttress thread	Reverse buttress thread
Cortical bone–implant interface	27.709	33.4226	26.9049	25.274
Cancellous bone–implant interface	1.51976	1.40778	1.99154	2.0288
Implant body	66.0093	50.433	54.01	50.9034
Overall stress	51.1821	53.8197	56.6273	45.865

Four separate FE constructs were developed and subdivided into nodes and tetrahedral solid components. The constructs were configured as:

1. A 10 mm long, 4 mm diameter implant incorporating V-shaped threads of 0.4 mm depth
2. A 10 mm long, 4 mm diameter implant incorporating square-shaped threads of 0.4 mm depth
3. A 10 mm long, 4 mm diameter implant incorporating buttress-shaped threads of 0.4 mm depth
4. A 10 mm long, 4 mm diameter implant incorporating reverse buttress-shaped threads of 0.4 mm depth
5. Simulated masticatory loading on the abutment components was executed by delivering 100 N in both axial and nonaxial (45°) trajectories.

Finite element analysis

Numerical simulation was conducted within the ANSYS software environment. The following response quantities were evaluated under 100 N axial and oblique loading regimes:

1. Global stress distribution across the models
2. Stress distribution prevailing at the cortical bone-implant boundary
3. Stress distribution prevailing at the cancellous bone-implant boundary
4. Stress arising inside the implant structure.

Von Mises stress within the designated zones was recorded and examined for each loading scenario. The compiled data appear in **Tables 3 and 4**.

Assessment of global stress under 100 N axial load

The V thread geometry yielded the uppermost magnitude of 19.451 MPa, while the reverse buttress thread geometry delivered the lowermost magnitude of 16.9331 MPa.

Assessment of global stress under 100 N oblique load

The buttress thread geometry yielded the uppermost magnitude of 56.6273 MPa, while the reverse buttress thread geometry delivered the lowermost magnitude of 45.865 MPa.

Assessment of cortical bone–implant interface stress under 100 N axial load

The buttress thread geometry yielded the uppermost magnitude of 9.43991 MPa, while the reverse buttress thread geometry delivered the lowermost magnitude of 8.26554 MPa.

Assessment of cortical bone–implant interface stress under 100 N oblique load

The square thread geometry yielded the uppermost magnitude of 33.4226 MPa, while the reverse buttress thread geometry delivered the lowermost magnitude of 25.274 MPa.

Assessment of cancellous bone–implant interface stress under 100 N axial load

The reverse buttress thread geometry yielded the uppermost magnitude of 2.4337 MPa, while the buttress thread geometry delivered the lowermost magnitude of 1.02297 MPa.

Assessment of cancellous bone–implant interface stress under 100 N oblique load

The reverse buttress thread geometry yielded the uppermost magnitude of 2.0288 MPa, while the square thread geometry delivered the lowermost magnitude of 1.40778 MPa.

Assessment of implant body stress under 100 N axial load

The buttress thread geometry yielded the uppermost magnitude of 17.8409 MPa, while the V thread geometry delivered the lowermost magnitude of 16.309 MPa.

Assessment of implant body stress under 100 N oblique load

The V thread geometry yielded the uppermost magnitude of 66.0093 MPa, while the square thread geometry delivered the lowermost magnitude of 50.433 MPa.

Conclusion

Dental implants are anchored wholly within the osseous tissue to take the place of the natural radicular structure and permit the attachment of a dental prosthesis [6]. The degree of primary stability secured at the moment of fixture insertion is linked to the extent of initial bone apposition. The quantity of bone-to-implant contact is influenced by a range of factors, including thread macrogeometry, operative protocol, and skeletal quality. Thread depth, thread thickness, thread face inclination, thread pitch, and thread helix angle all contribute to modulating the biomechanical load partitioning of the implant. Threads are engineered to optimize initial contact, boost primary fixation, augment implant surface area, and promote the dispersal of interfacial stress [5, 7, 8].

Within the scope of this work, three-dimensional FEA served as the investigative modality to examine and contrast the effects of a 0.4 mm thread depth across four different thread configurations on stress distribution at the bone-implant junction [9-11]. A geometrical replica of the mandibular posterior segment was reconstructed from CT imaging data. FE representations were subsequently produced. A force magnitude of 100 N, oriented both axially and nonaxially (45°), was homogeneously exerted upon the abutment for each of the four thread configurations. Given the loads imposed, the resulting stress contours were examined, and deductions were formulated [12-15].

The stress readings captured in the cortical and cancellous bone compartments were expressed as Von Mises stress. The most pronounced stress accumulations manifested within the implant structure itself relative to the bone-implant junction. Stress concentrations of greater intensity materialized at the cortical bone-implant boundary compared with the cancellous bone-implant boundary. The thread configuration that generated the severest stress concentration at the cortical bone-implant boundary produced the mildest stress concentration at the cancellous bone-implant boundary, and the opposite pattern was observed, irrespective of whether loading was axial or nonaxial [16-19]. The reverse buttress thread configuration gave rise to the mildest stress state at the cortical bone-implant boundary, yet the severest stress state at the cancellous bone-implant boundary under both axial and nonaxial loading regimes [20-22]. The buttress thread configuration gave rise to the severest stress state at the cortical bone-implant boundary and the mildest stress state at the cancellous bone-implant boundary under axial loading. The square thread configuration gave rise to the severest stress state at the cortical bone-implant boundary and the mildest stress state at the cancellous bone-implant boundary under nonaxial loading.

Acknowledgments: None

Conflict of Interest: None

Financial Support: None

Ethics Statement: None

References

1. Hobkirk JA, Havthoulas TK. The influence of mandibular deformation, implant numbers, and loading position on detected forces in abutments supporting fixed implant superstructures. J Prosthet Dent. 1998;80:169-74.
2. Ausiello P, Franciosa P, Martorelli M, Watts DC. Effects of thread features in osseo-integrated titanium implants using a statistics-based finite element method. Dent Mater. 2012;28:919-27.
3. Cook SD, Klawitter JJ, Weinstein AM. A model for the implant-bone interface characteristics of porous dental implants. J Dent Res. 1982;61:1006-9.
4. Vidyasagar L, Apse P. Dental implant design and biological effects on bone-implant interface. Stomatologija Balt Dent Maxillofac J. 2004;6:51-4.
5. Geng J, Ma X, Liu GR, Ying LA. The effect of element downsizing on finite element domains of infinite/finite element analysis in an implant-bone system. Int Chin J Dent. 2004;4:63-6.
6. Turkyilmaz I. Implant Dentistry - A Rapidly Evolving Practice [Internet]. Rijeka: InTech; 2011 [cited 2026 Jun 1]. doi:10.5772/706
7. Park JH, Lim YJ, Kim MJ, Kwon HB. The effect of various thread designs on the initial stability of taper implants. J Adv Prosthodont. 2009;1:19-25.
8. Steigenga J, Al-Shammari K, Misch C, Nociti FH Jr, Wang HL. Effects of implant thread geometry on percentage of osseointegration and resistance to reverse torque in the tibia of rabbits. J Periodontol. 2004;75:1233-41.
9. Van Staden RC, Guan H, Loo YC. Application of the finite element method in dental implant research. Comput Methods Biomech Biomed Engin. 2006;9:257-70.
10. Kong L, Liu B, Li D, Song Y, Zhang A, Dang F, et al. Comparative study of 12 thread shapes of dental implant designs: A three-dimensional finite element analysis. World J Model Simul. 2006;2:134-40.

11. Guda T, Ross TA, Lang LA, Millwater HR. Probabilistic analysis of preload in the abutment screw of a dental implant complex. J Prosthet Dent. 2008;100:183-93.
12. Bhatavadekar N. Clinical decisions and the quality of evidence available for dental implants. J Periodontol. 2009;80:1559-61.
13. Song DW, Lee DW, Kim CK, Park KH, Moon IS. Comparative analysis of peri-implant marginal bone loss based on microthread location: A 1-year prospective study after loading. J Periodontol. 2009;80:1937-44.
14. Chou HY, Müftü S, Bozkaya D. Combined effects of implant insertion depth and alveolar bone quality on periimplant bone strain induced by a wide-diameter, short implant and a narrow-diameter, long implant. J Prosthet Dent. 2010;104:293-300.
15. Abuhussein H, Pagni G, Rebaudi A, Wang HL. The effect of thread pattern upon implant osseointegration. Clin Oral Implants Res. 2010;21:129-36.
16. Faegh S, Müftü S. Load transfer along the bone-dental implant interface. J Biomech. 2010;43:1761-70.
17. Freitas AC Jr, Bonfante EA, Giro G, Janal MN, Coelho PG. The effect of implant design on insertion torque and immediate micromotion. Clin Oral Implants Res. 2012;23:113-8.
18. Kang YI, Lee DW, Park KH, Moon IS. Effect of thread size on the implant neck area: Preliminary results at 1 year of function. Clin Oral Implants Res. 2012;23:1147-51.
19. Orsini E, Giavaresi G, Trirè A, Ottani V, Salgarello S. Dental implant thread pitch and its influence on the osseointegration process: An in vivo comparison study. Int J Oral Maxillofac Implants. 2012;27:383-92.
20. Koticha T, Fu JH, Chan HL, Wang HL. Influence of thread design on implant positioning in immediate implant placement. J Periodontol. 2012;83:1420-4.
21. Chang JZ, Chen YJ, Tung YY, Chiang YY, Lai EH, Chen WP, et al. Effects of thread depth, taper shape, and taper length on the mechanical properties of mini-implants. Am J Orthod Dentofacial Orthop. 2012;141:279-88.
22. Kwon YS, Namgoong H, Kim JH, Cho IH, Kim MD, Eom TG, et al. Effect of microthreads on removal torque and bone-to-implant contact: An experimental study in miniature pigs. J Periodontal Implant Sci. 2013;43:41-6.